Conceptual Design of Superconducting Induction Motors Using $REBa_2Cu_3O_y$ Superconducting Tapes for Electric Aircraft

Koichiro Ozaki, Yuma Doi, Koichi Yoshida, Shun Miura, Teruyoshi Sasayama, Takashi Yoshida, Kaoru Yamamoto, Masataka Iwakuma, Akifumi Kawagoe, Akira Tomioka, Masayuki Konno, and Teruo Izumi

***Abstract*—High power density motors are required for electric propulsion aircrafts. The highest power density of the conventional motor is reported as 5.2 kW/kg up to now. Superconducting rotating machines have a potential to realize higher power density due to its high current density and a large magnetic field property. In this study, the induction motor with air-cored superconducting armature windings was conceptually designed. The output power range was 3 to 6 MW and the output power density aimed to be over 20 kW/kg. The armature voltage should be below kV-class and joule loss below 122 kW. The target efficiency was over 95%. The electromagnetic design and analysis were carried out by JMAG Designer. The number of magnetic poles and operating temperatures were set as two poles and liquid hydrogen temperature of 20 K, respectively. The parameter was power frequency in the range of 100–250 Hz. As a result, all the requirements were satisfied when the power frequency was 130 Hz. The feasibility of the MW-class superconducting induction motor was investigated, and in conclusion, the superconducting induction motor can be applied to the aircraft propulsion system.**

***Index Terms*—Superconducting coils, induction motors, aircraft.**

I. Introduction

EMISSIONS of CO_2 of fuel combustion have been increasing year by year [1]. The traffic of aircraft is predicted to about 2.4 times in next the 20 years, so the CO_2 emissions will increase further [2]. However, the ICAO and IATA aim to a 50% reduction in total aircraft CO_2 emissions in 2005 by 2050 [3]. The automotive industry has been moving to electric vehicles to reduce the CO_2 emissions. Analysis and design optimization of a motor and performance analysis of torque for an electric vehicle have been studied by [4]–[6]. In addition, the aircraft industry will be also becoming to be electrified. A distributed propulsion system with multiple fans is one of the promising solutions to reduce emissions by increasing efficiency. By the distributed propulsion, it is expected that the airframe can be designed as Blended Wing Body and then 72% of fuel can be reduced [7]. However, referring to NASA's conceptual design, we can see that these systems require a high output power density, especially for propulsive motors (>20 kW/kg). The world-record power density of conventional motor is ∼5.2 kW/kg [8], [9]. The distributed propulsion system requires about four times higher power density [10]. A superconducting technology has a potential to achieve such an extremely high power density requirement due to a capability of transporting a high current density and producing high magnetic field. In our previous studies, the synchronous fully superconducting rotating machines have been studied [11]–[13]. These machines need complicated structures as a rotating part with a slip ring for supplying electric power to field windings. From the viewpoint of dielectric strength and maintenance, the slip ring should be omitted. In this study, we studied superconducting induction motors for electric propulsion aircraft. The rotor is a cage rotor made of copper, and the stator is $REBa_2Cu_3O_y$ (REBCO) superconducting armature. Conventional motors usually use iron-core in the stators. Core losses are calculated by nonlinear lumped-parameter equivalent circuit model [14]. In this study, to achieve a high output power density, our induction motors employed air-core superconducting armature coils. The AC loss occurs in the superconducting armature windings due to AC magnetic field and current. Our research group has developed the laser-scribing technique and transposed parallel conductors to reduce the AC loss. These technologies were developed for superconducting transformers wherein the reduction of AC loss was successfully demonstrated [15], [16]. In addition, due to the strong magnetic field and high-speed rotation, a large Joule loss is expected to be produced in the copper rotor. The copper rotor is arranged outside the cryostat, with a fin cooled by outside air. Since the aircraft operates over 10 km above the sky, the air temperature is −50 °C and the speed over 800 km/h, so a high cooling effect is expected.

The purpose of this study is to conceptually design superconducting induction motors with output power of 3–6 MW with

Manuscript received September 24, 2019; accepted January 30, 2020. Date of publication February 5, 2020; date of current version April 3, 2020. This work was supported in part by the New Energy and Industrial Technology Development Organization, in part by the Japan Society for the Promotion of Science Grant-in-Aid-for Scientific Research under Grants JP18H03783 and JP19K14964, and in part by the Japan Science and Technology Agency: Advanced Low Carbon Technology Research and Development Program. *(Corresponding author: Koichiro Ozaki.)*

Yuma Doi, Kaoru Yamamoto, Koichiro Ozaki, Koichi Yoshida, Shun Miura, Teruyoshi Sasayama, Takashi Yoshida, and Masataka Iwakuma are with the Institute of Superconductors Science and Systems, Kyushu University, Fukuoka 819-0395, Japan (e-mail: ozaki@sc.kyushu-u.ac.jp).

Akifumi Kawagoe is with Kagoshima University, Kagoshima 890-0065, Japan.

Akira Tomioka and Masayuki Konno are with Fuji Electric Co. Ltd., Ichihara-city 290-8511, Japan.

Teruo Izumi is with the National Institute of Advanced Industrial Science and Technology, Tsukuba 305-8560, Japan.

Color versions of one or more of the figures in this article are available online at https://ieeexplore.ieee.org.

Digital Object Identifier 10.1109/TASC.2020.2971671

1051-8223 © 2020 IEEE. Personal use is permitted, but republication/redistribution requires IEEE permission.
See https://www.ieee.org/publications/rights/index.html for more information.

Authorized licensed use limited to: University of Exeter. Downloaded on May 07,2020 at 13:44:29 UTC from IEEE Xplore. Restrictions apply.

TABLE I
MAIN SPECIFICATIONS OF THE MODEL

Rotor diameter [mm]	256
Model diameter [mm]	370
Effective length [mm]	500
Winding configuration	Distributed winding and Full-pitch winding
Number of poles	2
Number of copper bars	20
Number of slots per phase per pole	2
Number of slots / phase	8
Slot thickness [mm]	4.5
Yoke thickness [mm]	20 (JSOL-50A230)
Total weight [kg]	145.8
Yoke weight [kg]	83.6
Copper weight [kg]	36.7
GFRP weight [kg]	21.9
EuBCO weight [kg]	3.54

a power density over 20 kW/kg. The efficiency target is 95% or more. The maximal voltage in armature windings should be set below kV-class due to low withstand voltage in the sky. By taking account of heat balance of joule heat and air cooling, two-dimensional numerical analysis was made for a steady-state situation with a software on the market, JMAG-designer.

II. Design of Superconducting Induction Motor

The REBCO superconducting tapes are developing by the National Institute of Advanced Industrial Science and Technology. The detailed electromagnetic properties were reported in the previous paper [11]. Here it is assumed that the REBCO superconducting wire will be laser-scribed into a 10-filament structure [17]. The AC loss of the REBCO tape was calculated by substituting the magnetic field amplitude penetrating vertically into the superconducting tapes into the approximate formula for the AC loss measured using a saddle-shaped pickup coil [18]. The magnetic field amplitude was analyzed using the finite element method. The refrigerant at the stator is assumed as liquid hydrogen at 20 K.

Table I shows the specifications of the induction motor. Fig. 1 shows a cross-sectional view in axis direction of the superconducting induction motor. The casing with a vacuum thermal insulation layer, bobbins for the superconducting windings and the shaft are made of GFRP. The GFRP wall of the casing was 4 mm in thickness and the vacuum layer of 6 mm in thickness. The electric gap between the inner diameter of stator and the outer diameter of rotor is 20 mm. The inset of Fig. 1 shows the size of copper rotor bars and copper fins for air cooling. The copper bar is 15 mm in height, 13.4 mm in innermost width, and 15.3 mm in outermost width. The number of copper bars was set as 20. The fin made of copper is attached to the copper bar, in order to increase cooling capacity. The length of the fin

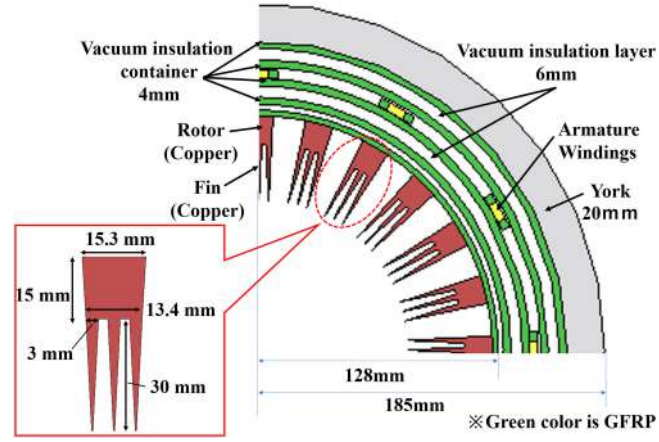

Fig. 1. 1/4 Sectional view in the Axial direction of the designed superconducting induction motor.

is 30 mm. Three fins are attached per a copper bar. The total weight was assumed as 145.8 kg. The heaviest part of the motor is the back iron yoke. It amounts to 57.3% (83.6 kg). The second heaviest part is copper rotor is 25.7% (36.7 kg).

The heat release was calculated using the convective heat transfer equation for a flat plate, for simplicity Ref. [19]. The copper bar and fin surfaces were assumed to be flat. Air at 800 km/h and -50 °C cools the rotor by forced convection. The heat dissipation amount Q from the surface of the flat plate is expressed by (1).

$$Q = \overline{h} LW \left(T_W - T_e\right). \tag{1}$$

$\overline{h}$ is the average heat transfer coefficient. L is the length of flat plate. W is the width of flat plate. T_w is the temperature of the flat plate. T_w is 150 °C. T_e is the temperature of the air. T_e is -50 °C. $\overline{h}$ is expressed by (2).

$$\overline{h} = \overline{N_{uL}} \frac{k}{L}. \tag{2}$$

$\overline{N_{uL}}$ is the Nusselt number that is a dimensionless number representing the ratio of heat transfer to heat transfer in a convective fluid. k is the thermal conductivity. k is 0.0276. $\overline{N_{uL}}$ is expressed by (3).

$$\overline{N_{uL}} = P_r^{1/3} \left(0.037 {R_{eL}}^{4/5} - 871\right). \tag{3}$$

R_{eL} is the Reynolds number that is dimensionless quantity defined by the ratio of inertial force to viscous force. R_{eL} is expressed by (4).

$$R_{eL} = \frac{u_e L}{v}. \tag{4}$$

u_e is the speed of air of 800 km/h in this study. v is kinematic viscosity of air in this paper. v is 0.00002976. P_r is the Prandtl number that is ratio of thermal energy diffusion to kinetic energy diffusion. P_r is expressed by (5).

$$P_r = \frac{\mu C_p}{k}. \tag{5}$$

Authorized licensed use limited to: University of Exeter. Downloaded on May 07,2020 at 13:44:29 UTC from IEEE Xplore. Restrictions apply.

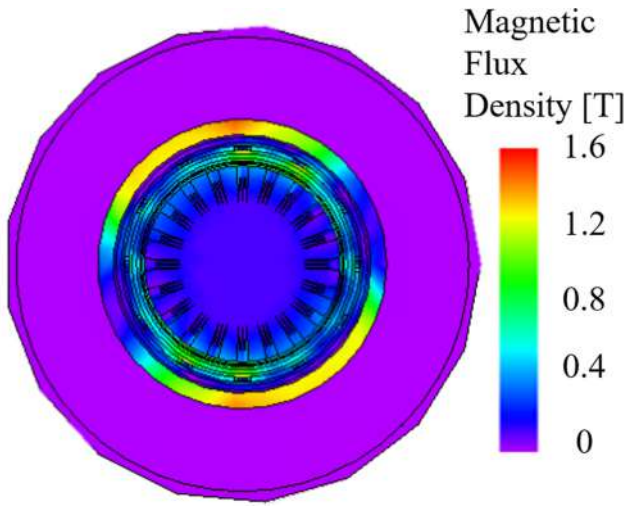

Fig. 2. Magnetic field distribution of the cross section of the induction motor when $T_{\rm op} = 20$ K and $f = 130$ Hz. $T_{\rm op}$ was set to the liquid hydrogen temperature of 20 K.

μ is viscosity coefficient. μ is 0.00001457. C_p is specific heat. C_p is 1005.

The calculated heat dissipation was 122.4 kW. In other words, the joule loss must be less than this heat dissipation amount.

III. Numerical Simulation of Superconducting Induction Motor

Fig. 2 shows the magnetic field distribution of the cross section of the induction motor at power frequency 130 Hz. The maximum magnetic field applied to the superconducting tape face in perpendicular was 0.1 T. The critical current at 20 K and 0.1 T-field was 1711 A. The stator current is 800 $A_{\rm peak}$, so the load factor was 46.8%.

Fig. 3 shows the output power vs slip frequency with various power frequencies. The range of the power frequency was 100–250 Hz. The slip frequency is expressed by (6).

$$f_s = Sf. \tag{6}$$

Where f_s is the slip frequency, S is the slippage. f is the power frequency. The solid lines show the output power properties. The dot lines show the torque properties. The maximum torque is 4671 Nm. All of the maximal output power is around the $f_s \sim 26$ Hz since the torque is maximum when the slip frequency is 32 Hz.

Fig. 4 shows joule loss (red line) and AC loss (blue line) for various power frequencies. These plots show the maximum output power for each power frequency indicated by the arrows in Fig. 3. The black dashed line is constraint condition of joule loss. Both joule loss and AC loss are roughly proportional to the power frequency. When the power frequency is less than 140 Hz, the induction motor can satisfy the required condition of the joule loss. For the power frequency of 150 and 200 Hz, the joule losses are almost the same values due to the same slip frequency as 26 Hz.

The voltage in armature windings is also proportional to the power frequency as shown in Fig. 5, since the impedance of the coil increases in proportion to the power frequency. When the power frequency is 100–150 Hz, the induction motor can satisfy the required condition of the armature voltage.

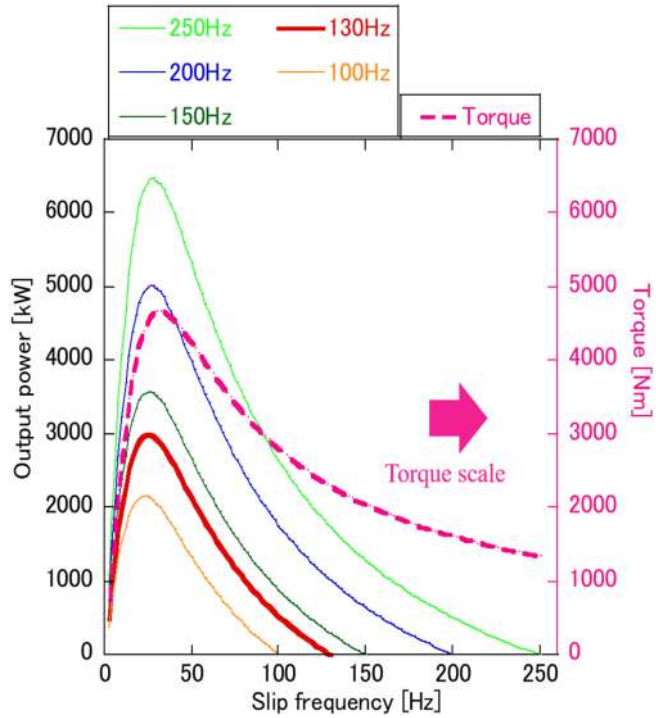

Fig. 3. Comparison of output power and torque by power frequency.

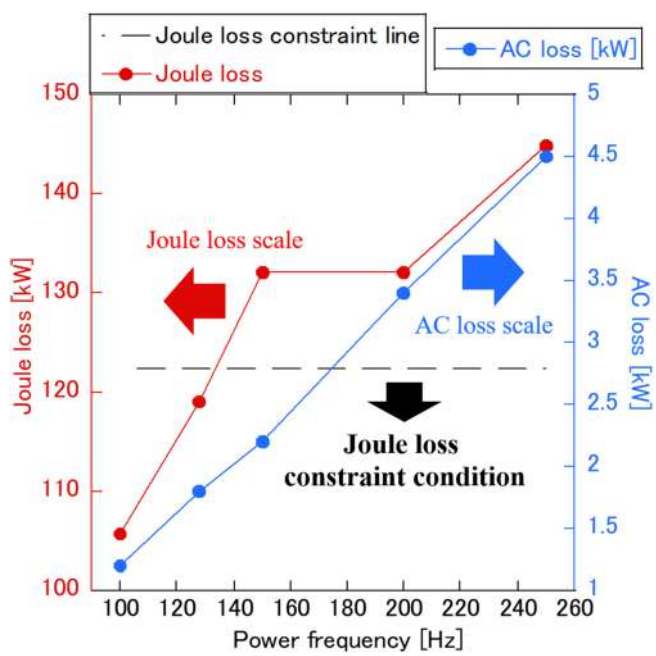

Fig. 4. Comparison of Joule loss and AC loss by power frequency.

The efficiency was calculated by (7).

$$\text{Efficiency} = \frac{\text{Output power}}{\text{Output power} + \text{AC loss} + \text{Iron loss} + \text{Joule loss}} \tag{7}$$

Authorized licensed use limited to: University of Exeter. Downloaded on May 07,2020 at 13:44:29 UTC from IEEE Xplore. Restrictions apply.

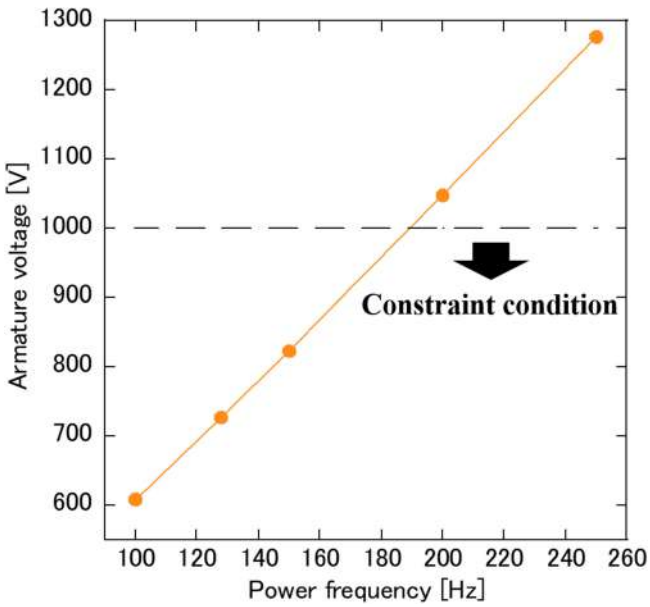

Fig. 5. Comparison of the voltage in armature windings by power frequency.

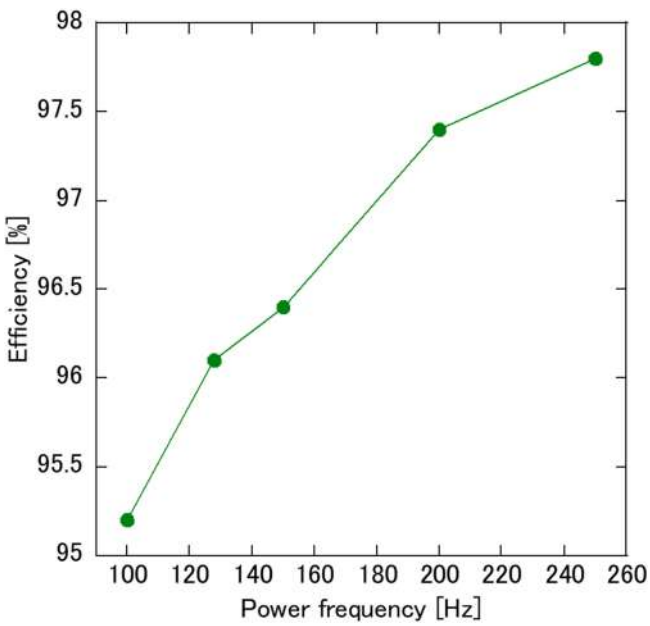

Fig. 6. Comparison of efficiency by power frequency.

After the use of the liquid hydrogen as a refrigerant, the hydrogen gas is used for fuel to the gas turbines. Therefore, the cooling penalty of cryocooler isn't included the efficiency calculation. The efficiency is also proportional to the power frequency as shown in Fig. 6. Table II shows the electromagnetic properties for the power frequency of 100–250 Hz. When the power frequency is 130, 150, 200 and 250 Hz, the induction motor achieved the output power density over 20 kW/kg. The efficiency of the designed motor achieved over 95% under all power frequency. When the power frequency is 100–150 Hz, the armature voltage was below 1 kV. The joule loss satisfied the heat dissipation requirement when power frequency are 100 Hz and 130 Hz.

TABLE II
ANALYSIS RESULTS

Power frequency [Hz]	100	130	150	200	250
Rotational speed[rpm]	4680	6360	7440	10440	13320
Armature voltage [Vpeak]	608	727	823	1048	1278
Armature current [Apeak]			800		
Number of turns per phase [turn]			120		
Torque [Nm]	4393	4506	4587	4587	4639
Power [kW]	2153	3001	3574	5015	6471
Weight [kg]			145.7		
Power density [kW/kg]	14.8	20.6	24.5	34.4	44.4
Iron loss[kW]	0.6	0.7	0.8	1.1	1.4
Joule loss [kW]	105.7	119.0	132.1	132.1	144.8
AC loss [kW] (10 scribing)	1.2	1.8	2.2	3.4	4.5
Efficiency [%]	95.2	96.1	96.4	97.3	97.7

IV. CONCLUSION

We conceptually designed 3 to 6 MW superconducting induction motor for electric aircraft and investigated the various properties for the frequency range of 100–250 Hz by numerical simulation. At the frequency of 130 Hz, the power density over 20 kW/kg, armature voltage less than 1 kV, efficiency over 95% and joule loss less than 122.4 kW were satisfied. As a result, the feasibility of MW-class superconducting induction motor was demonstrated. The output power and efficiency increased with power frequency.

In this study, the heat release from the copper rotor was calculated by the simple turbulent heat transfer equation assumed as a flat plate. In fact, more detailed heat calculations are required. For rotor rotational motion with respect to air convection, a two-dimensional model is not sufficient to obtain more accurate results. Therefore, three-dimensional thermal analysis is required to design an accurate ventilation system for an air-cooled induction motor [20].

The most of the weight was iron yoke (57%). One of the attractive solutions is using superconducting magnetic shield instead of iron yoke. The superconducting induction motors are expected to be drastically reduced the weight. However, the permeance of the magnetic path might decrease. Therefore, the generated torque might decrease, so it is necessary to investigate the superconducting magnetic shield in detail. Our research group has started to develop the superconducting shields.

REFERENCES

[1] IEA, "CO_2 EMISSIONS OVERVIEW," in *Proc. CO_2 Emissions from Fuel Combustion 2018 Highlights*, IEA, 2018, pp. 9–10.
[2] Airbus, "Demand for air travel," in *Proc. Global Market Forecast*, Airbus, 2018, pp. 18–19.

Authorized licensed use limited to: University of Exeter. Downloaded on May 07,2020 at 13:44:29 UTC from IEEE Xplore. Restrictions apply.

[3] P. Steele, "Aviation: Benefits beyond borders," IATA, May 2013, [Online]. Available: https://www.icao.int/Meetings/Green/Documents/DAY%202/Day%202%20PDF/MBM/4-Steele.pdf

[4] X. Sun, K. Diao, G. Lei, Y. Guo, and J. Zhu, "Study on segmented-rotor switched reluctance motors with different rotor pole numbers for BSG system of hybrid electric vehicles," *IEEE Trans. Veh. Technol*., vol. 68, no. 9, pp. 5537–5547, Jun. 2019.

[5] X. Sun, Z. Shi, G. Lei, Y. Guo, and J. Zhu, "Analysis and design optimization of a permanent magnet synchronous motor for a campus patrol electric vehicle," *IEEE Trans. Veh. Technol*., vol. 68, no. 11, pp. 10535–10544, Nov. 2019.

[6] X. Sun *et al.*, "Performance analysis of suspension force and torque in an IBPMSM with V-shaped PMs for flywheel batteries," *IEEE Trans. Magn.*, vol. 54, no. 11, Nov. 2018, Art. no. 8105504.

[7] S. W. Ashcraft, A. S. Padron, K. A. Pascioni, G. W. Stout Jr., and D. L. Huff, "Review of propulsion technologies for N+3 subsonic vehicle concepts," NASA, Tech. Rep. NASA/TM-2011-217239, 2011, Art. no. E-17995.

[8] Simens Press, "Siemens develops world-record electric motor for aircraft," Simens, Mar. 2015. [Online]. Available: https://press.siemens.com/global/en/pressrelease/siemens-develops-world-record-electric-motor-aircraft, Accessed on: Sep. 13, 2019.

[9] A. Makowska, "Electric propulsion components with high power densities for aviation," in *Proc. Symp. E2* –, Fliegen, 2015.

[10] A. K. Misra, "Technical challenges and barriers affecting turbo-electric and hybrid electric aircraft propulsion," NASA, Oral/Visual Presentation, Tech. Rep. GRC-E-DAA-TN48472, 2017.

[11] M. Komiya *et al.*, "Design study of 10 MW REBCO fully superconducting synchronous generator for electric aircraft," *IEEE Trans. Appl. Supercond.*, vol. 29, no. 5, Aug. 2019, Art. no. 5204306.

[12] S. Fukuda *et al.*, "Design study of 2-MW fully superconducting synchronous motors," *IEEE Trans. Appl. Supercond.*, vol. 28, no. 4, Jun. 2018, Art. no. 5207806.

[13] M. Iwakuma *et al.*, "Development of fully turbo-electric propulsion systems for aircrafts," presented at the CEC-ICMC2019, Hartford, USA, Jul. 2019.

[14] X. Sun, Y. Shen, S. Wang, G. Lei, Z. Yang, and S. Han, "Core losses analysis of a novel 16/10 segmented rotor switched reluctance BSG motor for HEVs using nonlinear lumped parameter equivalent circuit model," *IEEE/ASME Trans. Mechatronics*, vol. 23, no. 2, pp. 747–757, Apr. 2018.

[15] M. Iwakuma, H. Tanaka, and K. Funaki, "Experimental study on ac loss properties of two-strand parallel conductors composed of superconducting multifilamentary strands," *Supercond. Sci. Technol.*, vol. 15, 2002, Art. no. 1537.

[16] Y. Ohtsubo *et al.*, "Development of REBCO superconducting transformers with a current limiting function—Fabrication and tests of 6.9 kV-400 kVA transformers," *IEEE Trans. Appl. Supercond.*, vol. 25, no. 3, Jun. 2015, Art. no. 5500305.

[17] T. Imai, M. Okuyama, and Y. Hamakawa, "Development of scribing technique by using multiple-laser beams for multi-filamentary coated conductors," *J. Phys. Conf. Series*, vol. 1054, no. 1, Jul. 2018, Art. no. 012033.

[18] M. Iwakuma *et al*., "Theoretical investigation on the detection ratio of the magnetization in superconducting wires by a saddle-shaped pickup coil," *Supercond. Sci. Technol.*, vol. 16, no. 5, Mar. 2003.

[19] T. Bergman, A. Lavine, F. Incropera, and D. Dewitt, "External flow," in *Fundamentals of Heat and Mass Transfer*. WILEY, 2011, pp. 434–445.

[20] Y. Zhang, J. Ruan, T. Huang, X. Yang, H. Zhu, and G. Yang, "Calculation of temperature rise in air-cooled induction motors through 3-D coupled electromagnetic fluid-dynamical and thermal finite-element analysis," *IEEE Trans. Magn.*, vol. 48, no. 2, pp. 1047–1050, Feb. 2012.

Authorized licensed use limited to: University of Exeter. Downloaded on May 07,2020 at 13:44:29 UTC from IEEE Xplore. Restrictions apply.